Knocking on surfaces : interactions of hyperthermal particles with metal surfaces

Ueta, H.

Chapter 2

Scattering of Hyperthermal Argon Atoms from Clean and D-covered Ru(0001) Surfaces

Hyperthermal Ar atoms were scattered from a Ru(0001) surface held at temperatures of 180, 400 and 600 K, and from a Ru(0001)-(1×1)D surface held at 114 and 180 K. The resultant angular intensity and energy distributions are complex. The in-plane angular distributions have narrow (FWHM≤10°) near-specular peaks and additional off-specular features. The energy distributions show an oscillatory behaviour as a function of outgoing angle. These features, which are most visible when scattering from the clean surface at 180 K and from the Ru(0001)-(1×1)D surface, are consistent with rainbow scattering. The measured TOF profiles of the scattered atoms contain two components whose relative intensities vary as a function of the outgoing angle. This suggests two significantly different site and/or trajectory dependent energy loss processes at the surface. In comparison, scattered Ar atoms from a Ag(111) surface exhibits a broad angular intensity distribution and an energy distribution that qualitatively tracks the binary collision model. The results are interpreted in terms of the stiffness of the surface and highlight the anomalous nature of the apparently simple hcp(0001) ruthenium surface.

2.1 Introduction

Understanding the dynamics of atom and molecule scattering from surfaces provides knowledge useful in the development of applications involving processes such as sputtering, plasma etching and heterogeneous catalysis. However, detailed understanding at the molecular level can be hard to obtain because a variety of phenomena may occur simultaneously under process conditions. Understanding of simple systems is a gateway to the understanding of more complex ones. Therefore we study the interactions of inert gas atoms in this work as a prelude to studies with open shell atoms [1]. A variety of model systems involving the interaction of noble gas atoms with well-characterised sample surfaces have been used to investigate the specifics of energy exchange at surfaces [2-5]. It is well established that the interactions of noble gas atoms are physisorption mediated, involving a relatively shallow attractive well and a repulsive wall.

The scattering of atoms from surfaces can be divided into several regimes on the basis of the energy of the incident particle (E_i). For the thermal energy regime (E_i<1 eV), atoms generally see the surface as rather flat. In this situation scattering can be reasonably well described by the hard cube model, in which parallel momentum is conserved and only perpendicular momentum gets transferred to the cube [6]. When the particle energy exceeds thermal energy (hyperthermal regime), structure scattering will occur. In this regime, the interactions typically involve individual surface atoms. The simplest collision model to qualitatively describe atom scattering in this regime is the binary collision model between two hard spheres [5]. Previous studies have shown the transition between thermal and hyperthermal energy regimes [7, 8]. When a surface appears like a rippled mirror [9] or exhibits the individual surface atom corrugation surface rainbows may be observed [10]. At even higher particle energies of ten's to a few hundred eV, a number of ion scattering studies involving alkali ion-metal surface systems have been carried out [10-12], showing even more complex scattering processes.

To date, extensive studies involving noble gas atoms with hyperthermal energies scattering from metal [1, 7, 8, 13-24], semiconductor [14, 25-27] and graphite [28-31] surfaces have been performed. The Ar/Ru(0001) system has been investigated, using supersonic molecular beam techniques, for incident particle energies ranging from 0.08 to 2.32 eV [13]. The results were interpreted with reference to the washboard model [9] and trajectory calculations. At the high end of the energy range the angle-resolved energy of scattered Ar could be qualitatively described by the washboard model. Classical trajectory calculations did not describe the experimental results very well, although the correspondence could be improved by modifying the Debye temperatures. Quantum mechanical diffraction features were identified in the angular intensity distributions from the bare and H-covered Ru(0001) for Ar incident at energies of 80 and 65 meV respectively [13, 32]. Similar features were observed on the W(100)-2H surface [33, 34]. Subsequently, the Ru experimental results at 65 and 80 meV were compared with calculations involving a mixed quantum-classical

scattering theory [35-38]. The results were explained using an effective mass equivalent to 2.3 Ru atoms, implying collective effects of the target atoms in the Ru crystal.

In this chapter, the scattering of hyperthermal Ar atoms (average energy ~6.3 eV) from bare and D-covered Ru(0001) surfaces is presented. The current beam energy is significantly higher than in previously studies. By comparison with measurements from Ag(111) we gain insight into the nature of the Ru surface. The results shown in the following sections indicate the Ru(0001) behaves like a corrugated pseudo-static surface.

2.2 Experimental

The experiments were performed in an ultrahigh vacuum apparatus with a triply differentially pumped plasma source. The unique features of the apparatus have been described previously [1, 39, 40]. Briefly, the system contains a cascaded arc source [41, 42]. Ar (purity 99.999%) plasma is generated by discharge at three symmetrically-mounted cathode tips and is transported through a ∅=2.5 mm channel in a stack of 5 floating, mutually-isolated copper plates before expanding into the first vacuum stage of the beamline. The second stage of the beamline, which particles enter via a skimmer, contains a double slit (0.5% duty cycle) chopper in order to produce a pulsed beam, a beam flag to block the beam, and a pair of deflector plates in order to eliminate charged particles. The third stage functions as a buffer chamber.

The sample is mounted in the centre of the scattering chamber on a three-axis goniometer [43]. It can be moved aside, allowing measurement of the incident beam. The angular full width at half maximum (FWHM) of the direct beam is ~1.6°. This chamber contains an ion sputter gun, a residual gas analyser to monitor the background gas, and a differentially-pumped rotatable quadrupole mass spectrometer (QMS).

The Ru crystal used was oriented to within 0.1° of the (0001) face. The surface was cleaned by repeated cycles of Ar^+ sputtering follows by annealing to 1500 K for several minutes and then annealing for several minutes at 1200 K in an O_2 atmosphere (1×10^{-8} mbar). The final cleaning step was Ar^+ sputtering followed by annealing to 1500 K for several minutes and 1530 K flashing. The surface temperature (T_S) was monitored with a K-type thermocouple spot welded to the side of the crystal. The surface cleanliness was checked by reference to the temperature programmed desorption (TPD) spectra of CO and $H_2(D_2)$ [44, 45].

For the time-of-flight (TOF) experiments, the flight time of the Ar atoms was measured from the chopper to the rotatable QMS in the scattering chamber. Corrections for a trigger delay and the flight time of ions through the QMS have been applied to the raw data [1]. Note that, since the flight time of neutral particles with hyperthermal energy and the QMS ion flight time in our apparatus are of the same order of magnitude, failure to account for the ion flight time correctly would result in a substantial systematic error. The incident particle energy, final energies as a

function of scattering angle, and angular flux intensity distributions were all derived from TOF measurements after fitting with shifted Maxwell-Boltzmann distributions convoluted over the finite chopper opening time and over the spread of arrival times of particles at the surface [40, 46, 47].

In this study the incident Ar beams had an average energy ($<E_i>$) of ~6.3 eV. Our beams had a broad energy distribution ($E_{FWHM}/<E_i>$~0.98). The TOF spectra of scattered Ar were fitted with a combination of two shifted Maxwell-Boltzmann distributions. The motivation for fitting with two components is detailed in the following sections. Both components appear to be associated with scattering processes, since the slowest distribution is always much faster than a surface thermal energy distribution. The fits of the two components (each component having 3 fitting parameters) were unconstrained and independent of each other. After fitting and transformation from the time to energy domains employing the Jacobian and density to flux conversion (multiplication by v), a sum of scattered Ar energy distributions was derived. The average energies presented in this chapter are the mean values obtained from integration of these energy distributions (not the peak energy values).

In order to minimise the influence of adsorption from the residual gas (primarily H_2 and CO) during scattering from the bare Ru(0001) surface at T_S of 180 K and 400 K, the sample was flashed to 1530 K before each individual TOF measurement. The post-TOF coverage of these adsorbates was quantified by TPD. The coverages of CO were negligible and the final H coverage was <0.1 ML in all cases. For the experiments on the Ru(0001)-(1×1)D surface, the deuterium overlayer was prepared by background dosing at a partial pressure of 2×10^{-7} mbar D_2 (purity 99.8%) for 14 min. H(D) atoms preferentially bind in the fcc threefold-hollow sites [48]. The saturation coverage is unity relative to Ru surface atoms [49]. The resulting surface is quite inert to background contamination [50], such that several TOF spectra could be collected without requiring renewal of the surface.

2.3 Results

As mentioned in the experimental section, results of Ar scattering from bare Ru(0001) at T_S=180, 400 and 600 K, and from Ru(0001)-(1×1)D at T_S=114 and 180 K will be presented. All data points were obtained from analysis of individual TOF measurements. The data points in the angular intensity and the energy distributions were derived after conversion to flux sensitive intensity.

2.3.1 Angularly resolved intensity distributions

The in-plane intensity distributions arising from scattering of Ar incident at 40° (θ_i) with respect to the surface normal are shown in figure 2.1. Figure 2.1(a) shows the results for Ar scattering from the bare surface at the three different surface temperatures. Results from the D-covered surface are shown in figure 2.1(b). For comparison purposes, the angular distribution from the bare surface at T_S=180 K is

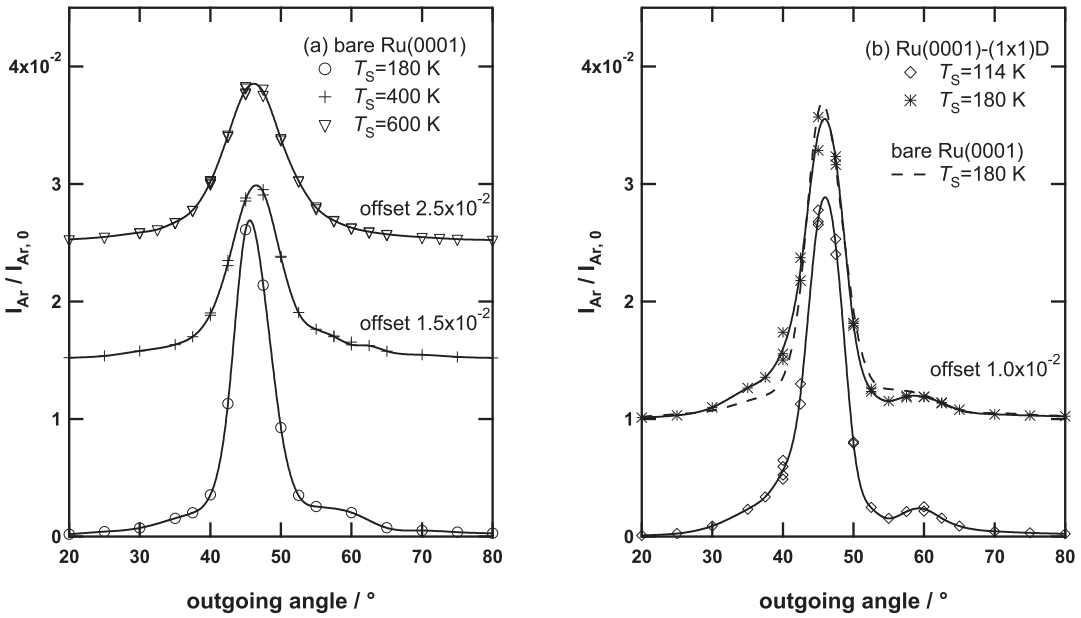

Figure 2. 1 Angle-resolved flux distributions of Ar atoms (<E_i>~6.3 eV; θ_i=40°) scattered from (a) Ru(0001) and (b) Ru(0001)-(1×1)D. The angular distribution from the bare surface at T_S=180 K is replotted in the panel (b) as a dashed line. The scattered intensities are normalised to the intensity of the corresponding direct beam. The lines connecting the data points are intended to guide the eye.

reproduced in this panel as a dashed line. All intensities shown are represented as a fraction of the corresponding direct beam intensity.

It can be seen in figure 2.1(a) that decreasing the surface temperature results in an increase in the peak intensity and a corresponding decrease in the FWHM of the angular distribution. The effect is relatively minor when the temperature is decreased from 600 K to 400 K, but is more pronounced when the temperature is further reduced to 180 K. In addition to the main peak, which has a temperature-independent maximum at a super-specular angle (θ_f~46°), the angular distribution at T_S=180 K has a shoulder at θ_f~60°. There is also an indication of a second shoulder at θ_f~35°.

The addition of D to the surface at T_S=180 K has no significant effect on the maximum intensity of the angular distribution. Further reducing the temperature of the D-covered surface to 114 K results in a small increase in the maximum intensity. The effect is on the same order of magnitude as was observed when T_S was reduced from 600 K to 400 K. The angular distributions at T_S=180 K and 114 K have almost identical features. The shoulder that is evident in the scattering from the bare surface at 180 K has resolved into a clear peak at θ_f~60° for both measurements from the D-covered surface. This peak is slightly more intense at T_S=114 K. There is also a significant increase in the intensity of the sub-specular wing of the angular distribution (θ_f=30°-40°) as compared with the bare surface, but this feature does not resolve into a distinct peak.

Figure 2.2(a) and (b) show the corresponding results for Ar scattering at θ_i=60°. Again the maximum intensity occurs at a super-specular angle (θ_f~65°). For the bare surface, the peak intensity of the angular distribution again increases with decreasing

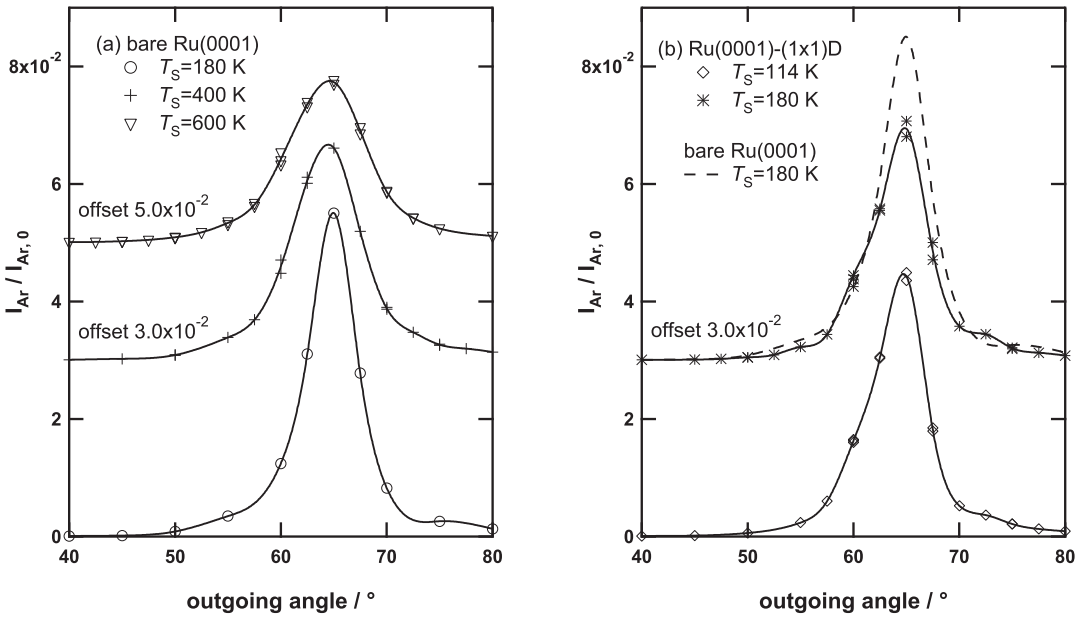

Figure 2. 2 Angle-resolved flux distributions of Ar atoms (<E_i>~6.3 eV; θ_i=60°) scattered from (a) Ru(0001) and (b) Ru(0001)-(1×1)D. The angular distribution from the bare surface at T_S=180 K is replotted in the panel (b) as a dashed line. The scattered intensities are normalised to the intensity of the corresponding direct beam. The lines connecting the data points are intended to guide the eye.

surface temperature. In this case, a substantial change is already observed upon decreasing from 600 K to 400K. Unlike the results obtained at θ_i=40°, adding D to the surface at 180 K results in a significant reduction in the peak intensity. This intensity increases again when the sample temperature is reduced to 114 K, but it remains lower than that measured from the bare surface at 180 K. As was the case for θ_i=40°, an additional shoulder/peak is evident at lower T_S along a super-specular scattering angle (θ_f~72°) and there is a wing on the sub-specular side of the main peak (θ_f=50°-55°).

2.3.2 Angularly resolved energy distributions

Figure 2.3 shows the results of our determination of the average energy of the scattered Ar on the basis of TOF measurements. Figure 2.3(a) and (b) show the angle-resolved ratios of the average final particle energy <E_f> over the average incident particle energy <E_i> for θ_i=40° as a function of θ_f. Figure 2.3(a) shows the results for the bare surface and figure 2.3(b) shows those for the D-covered surfaces, with the 180 K clean surface data reproduced for comparison purposes. The lines through the data points are intended to guide the eye. Two simple models are also included on the panels. The solid line that decreases as the outgoing angle increases represents parallel momentum conservation, while the dashed-dotted line that increases with outgoing angle represents the binary collision model for a single hard-sphere collision of the incident Ar from an isolated ruthenium atom (mass ratio m_{Ar}/M_{Ru}=40/101) [5].

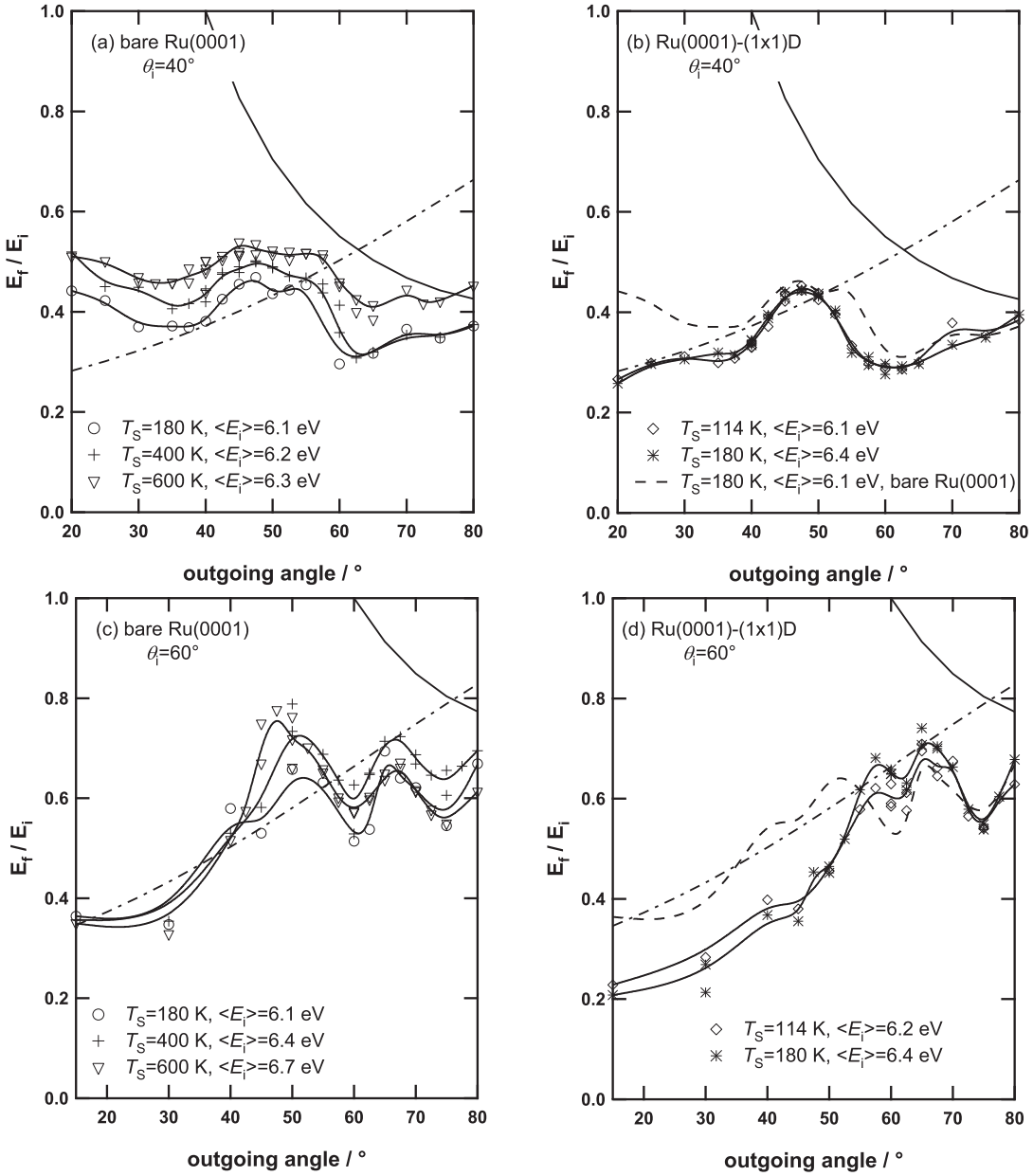

Figure 2. 3 Angle-resolved final-to-initial energy ratio (<E_f>/<E_i>) distributions of Ar atoms scattered from (a) Ru(0001) and (b) Ru(0001)-(1×1)D for θ_i=40°, and from (c) Ru(0001) and from (d) Ru(0001)-(1×1)D for θ_i=60° respectively. In (b) and (d) the results from the bare surface at T_S=180 K are replotted as a dashed lines. The lines connecting the data points are intended to guide the eye. Two simple models are illustrated on the panels. The solid lines correspond to parallel momentum conservation and dashed-dotted lines represent the model of single-collision hard sphere scattering of incident atoms from an isolated ruthenium atom (mass ratio of 40/101).

The energy ratios determined for the bare surface (figure 2.3(a)) show complex behaviour. <E_f>/<E_i> at a given θ_f is generally higher at higher T_S, but the overall shape of the distribution is temperature independent. If one were to apply a simple linear fit to the energy ratio curves in this panel, then the overarching trend would be of a gradual decrease as θ_f is increased. This is suggestive of a non-negligible contribution from parallel momentum conserving scattering events. However, this

trend is disrupted by a clear region of increased $\langle E_f \rangle / \langle E_i \rangle$ for θ_f between 40° and 60°. Adding D to the surface (figure 2.3(b)) results in two significant changes; the increase in the average energy now occurs over a narrower range of outgoing angles (θ_f=40°-50°) and there is a substantial decrease in the average energy of the particles scattered to small outgoing angle (which alters the overarching trend to one of increasing $\langle E_f \rangle / \langle E_i \rangle$ as θ_f increases). The latter behaviour was previously observed in the molecular beam study of Ar scattering from Ru(0001) and the effect was tentatively assigned to the influence of hydrogen (which was seeded in that beam) adsorption on the surface [13]. The current measurements confirm that this conjecture is correct.

Figure 2.3(c) and (d) show the corresponding datasets for θ_i=60°. At this incidence angle the energy distributions are even more complex. For the bare surface (figure 2.3(c)) the overall trend is one of increasing $\langle E_f \rangle / \langle E_i \rangle$ with increasing outgoing angle. This behaviour is qualitatively indicative of the binary collision model and suggests that any contribution from parallel momentum conserving scattering events is reduced at this incidence angle. However, two peaks (located at θ_f~50° and ~65°) are clearly evident in the energy distribution.

Adding D to the surface (figure 2.3(d)) again results in a decrease in $\langle E_f \rangle / \langle E_i \rangle$ at small outgoing angles, which is qualitatively similar to the behaviour observed at θ_i=40°. In addition, the peak structure is altered. While the peak at θ_f~65° is largely unchanged, the other peak has become less prominent and its maximum $\langle E_f \rangle / \langle E_i \rangle$ has shifted to θ_f~60°.

2.3.3 Comparison with results from Ag(111)

To highlight the unusual nature of the intensity and energy distributions measured from the Ru(0001) surface, it is instructive to compare the results with comparable measurements from the Ag(111) surface. This is done in figure 2.4, where the results of scattering from the two surfaces at T_S=600 K are presented. The results from the Ag(111) surface shown in figure 2.4 have been reported previously [1]. Although they have a different bulk structure, Ru (hcp) and Ag (fcc), have similar atomic masses (M_{Ru}=101 and M_{Ag}=108), and their respective (0001) and (111) faces have an equivalent top-layer atomic arrangement. The surface Debye temperatures have been reported as 216 K [51] for Ru(0001), and 155 K [52] and 165 K [53] for Ag(111).

Figure 2.4(a) and (b) show a comparison of the in-plane angular intensity distribution of scattered Ar from Ru(0001) and Ag(111) for θ_i of 40° and 60° respectively. The contrast is particularly dramatic at θ_i=40° where there is a factor of 4.6 difference in the maximum peak intensity. The angular distribution from Ru(0001) is much sharper than that from Ag(111) at both incident angles. At θ_i=40° the FWHM are ~10° and ~25° for Ru(0001) and Ag(111) respectively; at θ_i=60° the corresponding values are ~8.8° and ~13.3° (The QMS angular acceptance is ~1.6° assuming a point source at the sample position). Note that for this beam energy the Ag(111) FWHM value at θ_i=40° is broader than results reported for E_i in the range

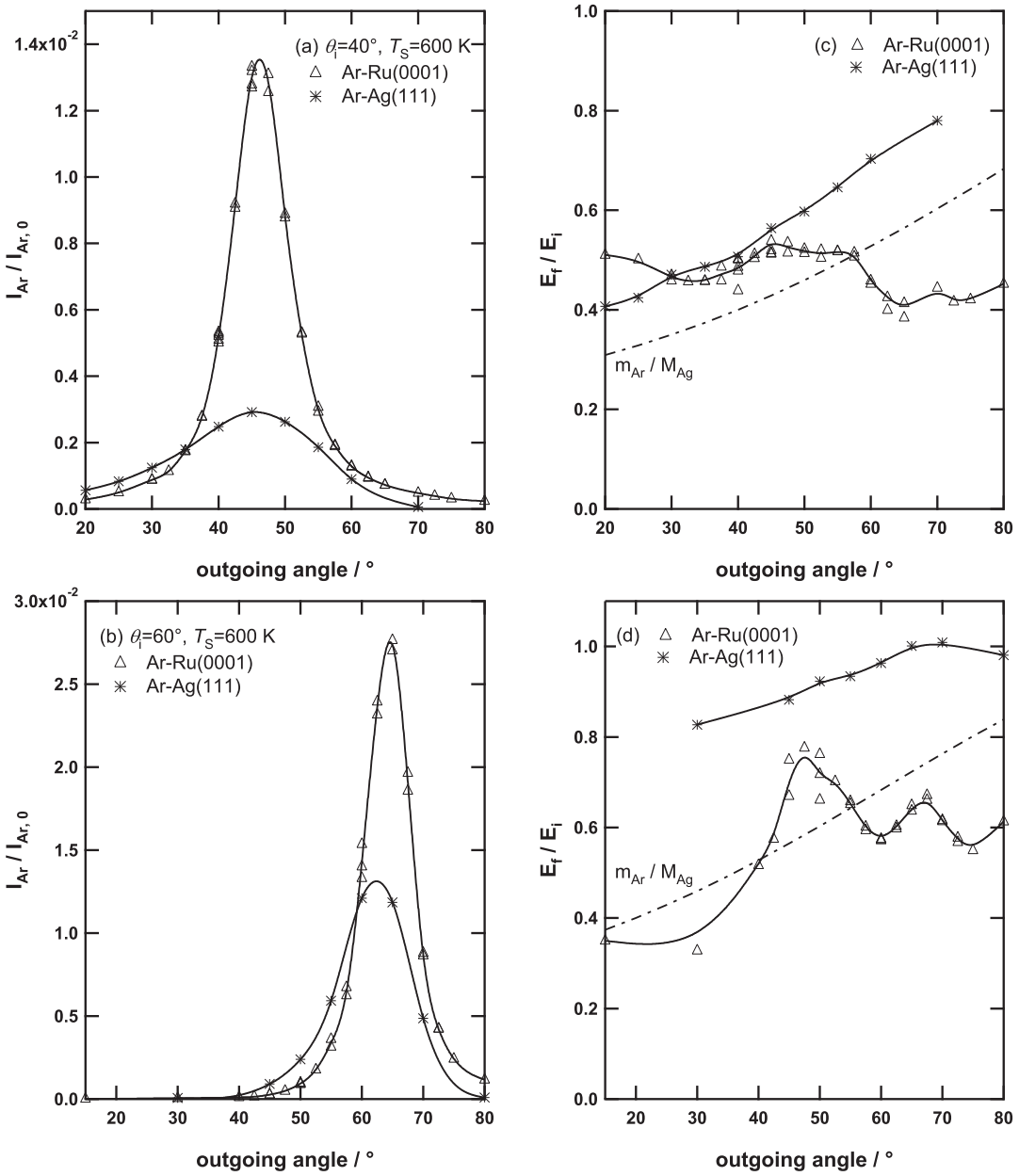

Figure 2. 4 Angle-resolved flux distributions of Ar atoms (<E_i>~6.5 eV) scattered from Ru(0001) and Ag(111) at (a) θ_i=40° and (b) θ_i=60°, and the corresponding angle-resolved <E_f>/<E_i> ratios from those surfaces at (c) θ_i=40°and (d) θ_i=60°. In panels (c) and (d), the dashed-dotted lines represent the models of single-collision hard sphere scattering of incident atoms from an isolated Ag atom (mass ratio of 40/108). The corresponding model for an isolated Ru atom are similar, but have a slightly lower <E_f>/<E_i>.

0.5-2.6 eV [7, 23], while the Ru(0001) FWHM is comparable to a previous result (~11°) for E_i=2.09 eV under a similar experimental conditions (T_S=550 K) [54].

Figure 2.4(c) and (d) show the corresponding comparison of <E_f>/<E_i> as a function of outgoing angle. The <E_f>/<E_i> ratios of Ag were previously determined on the basis of fitting a single shifted Maxwell-Boltzmann distribution to the scattered TOF spectra [1]. In figure 2.4(c) and (d) these ratios has been recalculated on the basis of the two-component fitting outlined in the experimental section. This was done to

ensure equivalent treatment of all datasets. In the case of Ag(111), the extra component results in a small improvement in the quality of the overall fit to the slow tail of the TOF spectra. As a consequence, the $<E_f>/<E_i>$ derived are slightly lower than those determined using a single component fitting.

The simplicity of the Ag(111) energy distributions is in stark contrast to the complexity of the corresponding Ru(0001) distributions. For both incidence angles the $<E_f>/<E_i>$ of Ar scattered from Ag(111) increases with increasing θ_f. The trend is qualitatively very similar to the simple binary collision model, although at both incident angles the average final energy ratio is higher than would be expected from that simple model. The deviation from the m_{Ar}/M_{Ag}=40/108 model is largest for θ_i=60°. The results can be interpreted either in terms of the effective mass of the surface being larger than the atomic mass of a single Ag atom (scattering from a collective mass) or by the scattering being dominated by multiple forward collisions [55, 56].

The $<E_f>/<E_i>$ determinations for Ar scattering from Ru(0001) at T_S=600 K are far more complex than those of Ag(111). Superficially, the measured final energies fall in the vicinity of the single Ru atom binary collision model. The values determined for θ_i=40° are in relatively good agreement with this model for θ_f near the specular angle. However, as noted above, the $<E_f>/<E_i>$ of scattered Ar for θ_i=40° has an overall decreasing trend as a function of θ_f that is indicative of parallel momentum conservation. In the case of θ_i=60° the data is close to the binary collision model at small θ_f. For both incidence angles, $<E_f>/<E_i>$ drops below the binary collision at large θ_f. This could imply trajectories involving multiple hard collisions or interactions involve substantial inelastic loss processes. In both cases the oscillations of $<E_f>/<E_i>$ as a function of θ_f are incompatible with any simple collision model.

2.3.4 Two-component TOF distributions

In the previous study of Ar and N scattering from Ag(111) the measured TOF spectra were analysed by fitting a single shifted Maxwell-Boltzmann distribution [1]. The resultant fits were sufficient to accurately represent the data. The main discrepancy was in the correspondence of the fit to the tail (slow component) of the TOF spectra. There was no significant variation in the quality of the single component fit as a function of θ_f. In contrast, in the case of the Ru TOF measurements, and in particular for certain outgoing angles, a single component fit was clearly insufficient to accurately represent the spectra. This is illustrated by figure 2.5(a-c), which compares three contour plots, each constructed from sets of individually measured TOF spectra. In all cases, the raw spectra at the individual outgoing angles have been normalised to a peak intensity of one.

Figure 2.5(a) shows the contour plot for scattering of Ar from Ag(111) at θ_i=40° and T_S=600 K. This shows an essentially constant time profile as a function of θ_f. The peak of the distribution shifts to shorter time as θ_f increases, which reflects the smoothly increasing $<E_f>/<E_i>$ shown in figure 2.4(c). In other respects the

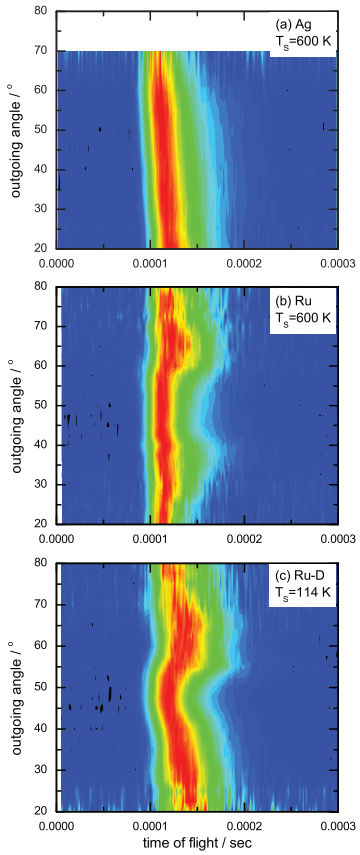

Figure 2. 5 Contour plots of Ar TOF spectra. The individual spectrum have been normalised to a peak intensity of one: (a) Ar scattered from Ag(111) at θ_i=40° and T_S=600 K; (b) Ar scattered from Ru(0001) at θ_i=40° and T_S=600 K; (c) Ar scattered for scattering from Ru(0001)-(1×1)D at θ_i=40° and T_S=114 K.

distributions do not vary dramatically. The shape and width of the distribution and the relative contribution from any slow component are effectively independent of the outgoing angle.

Figure 2.5(b) shows the equivalent contour plot for scattering of Ar from Ru(0001) at θ_i=40° and T_S=600 K. It is immediately clear that the time profile of the TOF distributions is no longer has a simple dependence on θ_f, and that it is now composed of two components. The slower component either appears or has a greatly enhanced relative contribution to the TOF spectra at certain outgoing angles: specifically for the θ_f=30°-40° and θ_f=60°-70° regions. The variation in the contribution from this component as a function of θ_f is the primary cause of the oscillations in $\langle E_f \rangle / \langle E_i \rangle$ evident on figure 2.3(a).

Figure 2.5(c) shows the contour plot for scattering of Ar from Ru(0001)-(1×1)D at θ_i=40° and T_S=114 K. Under these conditions the variations in the time profile of the TOF spectra as a function of θ_f are even more extreme. The shape of the associated T_S=114 K $\langle E_f \rangle / \langle E_i \rangle$ trace (shown on figure 2.3(b)), is clearly discernable in the angular variation of the contour maximum. Under these conditions the relative

contribution from the slow component is much greater at certain outgoing angles than was the case at T_S=600 K.

2.4 Discussion

Noble gas scattering behaviour is determined by the physisorption potential well, the shape of the potential, the target mass (effective mass) and by the thermal motion of individual surface atoms. These can be modified by the presence of hydrogen.

We first consider the influence of hydrogen on the surface physisorption well. The well depths of the bare and H-covered surfaces are approximately 65 meV and 69 meV respectively [57]. Although the H-covered surface is slightly more attractive than the bare surface, we consider that the difference will have a negligible effect on atoms impinging with hyperthermal energies. Consequently, in the current study the interaction between the Ar atoms and the different surfaces should be dominated by the repulsive wall. Considering the target mass, the mass of a D atom is negligible when compared with that of a Ru atoms. However the effective surface mass might be changed by modification of the repulsive wall. For the influence of phonons, we can compare the surface Debye temperatures of bare and H-covered Ru(0001), which have been reported previously. The value of the surface Debye temperature increases by 10% when H is added to the surface [57]. Surface phonon dispersion curves of bare and H-covered surface obtained by high resolution He scattering imply that the surface Debye temperatures are very similar, but that H may change the repulsive part of the potential [58].

2.4.1 Ar scattering from Ru(0001): Angular distributions

For the angular intensity distributions, the surface temperature dependence observed from Ru(0001) is qualitatively understandable in terms of the influence of temperature on surface atom motion. Raising the temperature increases the vibrational amplitude and displacement of the surface atoms, which will reduce the intensity of the specular peak and broaden the distribution. Nonetheless, the angular distributions remain surprisingly narrow compared with those measured from Ag(111). The additional peaks/shoulders at super- and sub-specular angles are enhanced when the surface temperature is reduced and in particular when D is added to the surface. Since reducing the temperature results in dampening of atomic motion, this suggests that D adsorption acts to suppress the motion of individual surface atoms.

With increasing energy, atoms probe deeper into repulsive wall. For hyperthermal particles, it is possible to observe surface rainbow scattering [10]. However, vibrations and thermal displacement of surface atoms typically act to wash out rainbow features in most scattering systems. This effect was simulated by Lahaye *et al.* for Ar scattering from static (T_S=0 K) and T_S=600 K Ag(111) surfaces with an incident angle of 40° [23]. Rainbow features at different outgoing angles were readily evident from the static surface for incident atoms with energies ranging from 0.1 eV

to 100 eV. In contrast, for the simulations done at T_S=600 K all surface rainbow features disappeared due to thermal effects. Ar with E_i=1 eV scattered from the static surface exhibited surface rainbow features at θ_f~35° and ~55° with a sharp main (split-)peak centred at ~45°. The central (near specular) peaks of the angular distribution were attributed to centre-site scattering and a small number of atop scattering events. The outer rainbow peaks consisted of atoms scattered from the surroundings of the atop site (the "up-hill" potential scattered to small θ_f and the "down-hill" potential to large θ_f).

For E_i=10 eV, the rainbow scattering features remained visible and the splitting of the central peak was clearly resolved. The positions of the two left-hand-side (small θ_f) peaks shifted to smaller θ_f with increased E_i. Since a collision with the up-hill potential is akin to a head-on collision with a single surface atom, the final θ_f is very sensitive to the E_i of the Ar and shape of the potential energy surface (PES). Conversely, the two rainbow peaks at larger θ_f (arising from collisions with the down-hill potential) did not shift significantly when E_i increased from 1 eV to 10 eV. These interactions are grazing and tended to scatter atoms along the surface, thus increasing the probability of a second collision with a surface atom. Such double collisions compensated for the energy-dependent variation in the shape of the PES and made θ_f independent of E_i.

The current angular intensity distributions for θ_i=40° at low T_S, and in particular from the D-covered surface, have clear shoulders/peaks at θ_f=30°-40° and θ_f=55°-65°. These features are qualitatively reminiscent of the simulation results for the static Ag(111) surface, in particular those of simulation at E_i=1 eV (see figure 3(a) and (b) of Lahaye *et al.* [23] and also figure 1.3 in this thesis). Note that given our broad energy distribution, the 1 eV and 10 eV simulations represent reasonable lower and upper limits of the spread of particle energies present in our beam. Ar atoms with energies between these values account for ~90% of the total beam. A broad range of incident E_i should result in the rainbow peaks at small θ_f (which have an energy dependence) being smeared over a range of θ_f, while those at lager θ_f (which are energy-independent) remains relatively sharp and well-defined peaks.

The angular distributions from D-covered Ru(0001) are compatible with this expectation. The central peak is sharp on the high θ_f side but broadened on the low θ_f side. This is consistent with it being an amalgamation of two rainbow peaks: one (right-hand side/larger θ_f) being energy independent and the other (left-hand side/small θ_f) shifting as a function of the incident particle energy. Considering the two outer rainbow features in the data from Ru(0001), there is a reasonably well-defined peak at θ_f~60° in contrast to a broad shoulder at θ_f=30°-40°. The fact that the peak at θ_f=60° is visible despite the broad energy distribution of the incident beam indicates that it is an energy-independent feature. The shoulder at small θ_f may be the net result of the smearing of an energy-dependent left-most rainbow peak. Based on the correspondence between the simulated Ar/Ag(111) and our measured angular distributions from Ru(0001), the low T_S and D-covered Ru appear to behave like

pseudo-static surfaces, with the consequence that associated rainbow features remain discernable under experimental conditions.

As mentioned above, the simulation results for Ar scattering from Ag(111) at T_S=600 K suggest that surface rainbow effects get washed out due to displacement of atoms from their equilibrium positions and the actual vibration of surface atoms. In order to separate those two effects, Lahaye *et al.* simulated Ar scattering from a surface with no thermal energy but with the atomic positions displaced according to a typical 600 K distribution [23]. They found that this displacement was sufficient to wash out the rainbow features, even in the absence of thermal vibrations. Thermal displacement of Ru atoms and the associated kinetic energy of vibration should also attenuate rainbow scattering features in a similar manner. Despite this, the angular intensity distributions from Ru(0001) at T_S=600 K remain much sharper than that from Ag(111) and remnants of the rainbow features, though less obvious at this temperature, persist in the angular distribution. This implies that the Ru surface has a much lower atomic displacement and is markedly stiffer (smaller vibrational amplitude) than the Ag surface.

Based on the reported surface Debye temperatures, the estimated root mean square displacements at T_S=600 K of Ag(111) and Ru(0001) in the harmonic approximation [59] are 0.17-0.18 Å and 0.14 Å respectively. These values indeed indicate smaller thermal displacement of Ru atoms, although the absolute difference between Ag and Ru does not seem to be dramatic. Ru displacement will be reduced both by lowering the temperature and by adding hydrogen to the surface. The root mean square Ru atomic displacement at a surface temperature of 180 K is estimated to be ~0.075 Å, based on a surface Debye temperature of 216 K in the harmonic approximation. With a 10% increase in the surface Debye temperature upon hydrogen adsorption [57], the root mean square displacement becomes even less, and surface atoms will be located even closer to their equilibrium positions.

It should be noted that there is a large disparity in the values of the Ru bulk Debye temperature that have been reported (415-600 K) [60-62]. These values are generally higher than those of the other transition and of the noble metals. Based on the bulk values reported and associating the single reported value for the Ru surface Debye temperature (216 K [51]) with the lower limit, then corresponding range of Ru surface Debye temperatures would approximate to 216-312 K. Any increase in the surface Debye temperature translates into a reduced root mean square displacement at a given temperature.

Tentative support for a higher than reported Ru surface Debye temperature is provided by the efforts of Berenbak *et al.* to simulate the results of their molecular beam measurements on the Ar/Ru(0001) system [13]. Calculations done on the basis of bulk and surface Debye temperatures of 415 K and 216 K respectively were not satisfactory in reproducing the experimental results. However, the level of agreement was improved by increasing the Debye temperatures in their trajectory calculations. An increase of a factor of 1.5-2.0 resulted in the calculations exhibiting energy

distribution trends that were qualitatively similar to the experimental results and to the washboard model.

The features observed for Ar scattered from Ru at θ_i=60° at low T_S and with D added to the surface are reminiscent of those at θ_i=40°. The central peak is broader on the small θ_f side than on the large θ_f side. There is also evidence of additional features at both smaller and larger θ_f. Although the feature on the large θ_f side of the main peak does not fully resolve into a distinct peak, it is more evident than the wing on the small θ_f side. This is again indicative of the features at larger θ_f being more independent of the incident particle energy than the features at smaller θ_f.

2.4.2 Ar scattering from Ru(0001): Energy distributions

As outlined above, the features of the angular distributions at θ_i=40°, particularly those measured for low T_S, are qualitatively similar to the simulations of Ar scattering from the static Ag(111) surface. The shapes of the corresponding energy ratio curves in current study also have similarities to the results of Lahaye *et al.* from static Ag(111) surface for E_i=1 and 10 eV [23], although the measured values of $\langle E_f \rangle / \langle E_i \rangle$ for Ru(0001) are consistently lower than the simulation. For these incident energies the simulations show an increase in relative energy between the outgoing angles of 40° and 50° (described as a 'kink'). A similar kink is evident in the average energy distributions shown in figure 2.3(a) and (b). Note that the width and position of the energy kink measured for the D-covered Ru surface is in very good agreement with that reported by Lahaye *et al.* for the static Ag(111) surface. In contrast to the rainbow features observed in the measured angular distributions, which get more washed out at elevated T_S, the energy kink remains clearly evident even at T_S=600 K.

Lahaye *et al*. identified this feature as arising from trajectories with reduced energy loss resulting from zig-zag collisions through the centre site [23]. The presence of D in the threefold-hollow sites can be expected to modify features associated with trajectories through such sites. This is indeed what is evident in figure 2.3(b), where the presence of D modifies (decreases) the width of the measured energy kink. The other major change that is induced by the addition of D is a drop in $\langle E_f \rangle / \langle E_i \rangle$ at small θ_f. This suggests that the small number of Ar atoms that are scattered in this direction arise primarily from trajectories associated with the threefold-hollow sites.

The preceding discussion, which relates to the energy distributions measured at θ_i=40° should also be applicable to the corresponding measurements for θ_i=60°. Unfortunately, comparable static surface trajectory calculations for this angle of incidence are not currently available, so no judgement can be made regarding the level of agreement. Assuming the trajectory associations identified based on the θ_i=40° simulations also hold at θ_i=60°, then the features that change upon adsorption of D (more energy loss at small θ_f and modification of the peaks) should also be assigned to centre site scattering trajectories. More detailed discussion of the oscillations seen for θ_i=60° is difficult in the absence of supporting trajectory calculations.

Rainbow features in energy-resolved scattering of atoms with hyperthermal energies have previously been reported experimentally and theoretically [63, 64]. The structures observed in the energy distributions shown in figure 2.3 may also be related to rainbow scattering. As illustrated by figure 2.5, the variations in E_f as a function of θ_f arise from changes in the relative contribution of two components in the TOF profiles, rather than from an angle-dependent variation in the energy of a single component. Clearly the TOF distributions contain significant contributions from two independent sets of trajectories. The fact that these two sets remain identifiable, rather than being washed out by thermal effects, is again indicative of scattering from a relatively static surface.

In order to exhibit two distinct components, different sites on the Ru surface must generate in-plane scattering trajectories that have very different energy losses. This points to an impact-site-dependent energy loss, such as was reported for the Ar/Pt(111) system with hyperthermal incident energies [24]. Note that the slower components appear to be most prominent at the outgoing angles associated with the outer-most features evident in the angular distributions. Based on the assignment of Lahaye *et al.* these features are due to scattering from the surroundings of the atop site (up- and down-hill potential), trajectories that are likely to be dominated by interactions between individual atomic cores and are thus more likely to experience a lower effective surface mass (higher energy loss). The zero temperature calculations of Kulginov *et al.* illustrate that scattering from a static surface can indeed lead to multiple values of $\langle E_f \rangle / \langle E_i \rangle$ along a single θ_f [22]. The shape and magnitudes of the energy losses calculated varied with the surface corrugation. Kulginov *et al.* identified the lower branches of their $\langle E_f \rangle / \langle E_i \rangle$ curves as being associated with scattering from a single surface atom, while the upper branch was due to simultaneous interaction with multiple atoms near the hollow sites.

As can be seen in figure 2.4(c) and (d), the absolute values of the energy ratios as a function of θ_f for scattering from Ru are closer to the single mass binary collision model than the comparable values from Ag. In some cases the final energy of the Ar/Ru data is even lower than that model, especially at large θ_f. With increasing energy, Ar atoms see a more corrugated PES and fewer surface atoms contribute to the repulsion at the turning point. Hence, the particles incident with the highest energy should "feel" the lowest effective surface mass. However, in the binary collision limit for elastic scattering the effective mass should not become lower than the mass of the surface atoms.

It is possible that additional loss processes may be operative on the Ru(0001) surface. Previously, excitation of electron-hole pairs at the surface of the Ar/Pt(111) system was suggested to explain the discrepancy between measured and calculated energy transfer during scattering of Ar atoms in a high energy regime ($E_i \cos^2 \theta_i > 3$ eV) [22]. If electron-hole pair creation also occurs during the Ar interaction with Ru(0001), it would result in additional energy transfer. However, since both Ag and Ru are metals and the surface work function of Ru(0001) is higher by about 0.7 eV [65, 66], it is again difficult to explain the difference in results from Ru(0001) and Ag(111)

solely on such a basis. One possible reason for the unusually low $\langle E_f \rangle / \langle E_i \rangle$ values determined for the Ru surface is the inter-play of the broad energy profile of our incident beam and out-of-plane scattering. In a follow-up paper, Lahaye *et al.* reported on the out-of-plane results of Ar scattering from Ag(111) (static and T_S=600 K) [67]. Since there is a good correspondence between our measured in-plane distributions and the simulations for the static surface, a similar correspondence in the out-of-plane scattering should be anticipated. The general trend observed by Lahaye *et al.* was that the extent of out-of-plane scattering increased with E_i. Applying such a trend to our broad-energy beam implies that the particles that are scattered in-plane will be preferentially weighted in favour of the lower energy incident particles. Hence, the energy distribution of the in-plane particles may not retain a simple direct correspondence with the energy distribution of the incident particles. The effect would be to reduce $\langle E_f \rangle / \langle E_i \rangle$. Note that this can only be an issue for beams with a broad energy spread; energy ratios determined with a mono-energetic beam cannot be distorted by out-of-plane scattering. Due to the possible distortion by the energy-dependent nature of out-of-plane scattering, the absolute values of $\langle E_f \rangle / \langle E_i \rangle$ determined using our incident beam should be treated with caution. However, conclusions can still be drawn on the basis of relative comparisons.

The unique features in the angular intensity and energy distributions measured, and their apparent similarity with static surface simulations point to a remarkable stiffness of the Ru surface. This is consistent with previous reports on the nature of the Ru(0001) surface. The surface lattice dynamics of Ru(0001) were studied by Heid *et al.* [68, 69]. They found evidence of a strong softening of longitudinally-polarized vibrations, which was attributed to a very large softening of the intra-layer coupling in the outermost atomic layer. This softening is in contrast to a substantial strengthening of the first-to-second inter-layer coupling. These are quite anomalous features as compared with other metals surfaces. A strong inter-layer coupling and a weak intra-layer coupling supports the suggestion by Hayes *et al.* that the effective mass of the Ru surface is dominated by the interaction of first layer atoms with the second layer [35, 36]. Such a substantial difference between inter- and intra-layer coupling strength, giving rise to large site and trajectory dependent variations in the net energy loss, could result in the bimodal TOF distributions that we measured. The energy loss may vary depending on whether the induced displacement of the surface atoms is primarily lateral with or perpendicular to the surface atomic plane. Perpendicular displacement can be anticipated to represent the maximum distortion of the strong inter-layer coupling, leading to the highest effective mass and the lowest energy loss. However, since all atomic displacement will involve some perturbation of all atomic couplings, the energy loss associated with any given displacement is not inherently obvious. Trajectory calculations using an appropriately modelled surface are necessary in order to elucidate the link between specific Ru atom displacements and the associated energy loss by incident Ar.

2.5 Conclusions

Results for both the angular flux and energy distributions of Ar scattering from Ru(0001) are qualitatively closer to simulation results for a static Ag(111) surface than to those from a surface at T_S=600 K. Rainbow scattering features are visible in both the angular flux and energy distributions measured from Ru. The rainbow features are enhanced by reducing the surface temperature and by adding D to the surface; both of which act to reduce surface atomic motion. The results point to a remarkable stiffness of the Ru surface. That Ru can be expected to be "stiffer" than other metal surfaces is indicated by its higher Debye temperatures, but the effect appear to be much more pronounced than might be anticipated be on the basis of the differences in the reported values of Debye temperatures. Previous efforts to interpret scattering data from Ru(0001) surfaces have encountered difficulty in adequately explaining the complexity of the measurements and in producing a satisfactory correspondence with simulations. Based on the current study, we propose that the difficulties arise as a result of treating the Ru surface too much like a "normal" metal. In particular, attention should be paid to properly accounting for the pronounced difference in the strengths of intra-layer and inter-layer atomic coupling. The uniqueness of the Ru(0001) surface could prove immensely valuable in refining modelling of atomic scattering and in improving the correspondence between simulation and experiment.

Bibliography

[1] H. Ueta, M.A. Gleeson, A.W. Kleyn, The Journal of Physical Chemistry A, **113** (2009) 15092-15099.
[2] J.A. Barker, D.J. Auerbach, Surface Science Reports, **4** (1984) 1-99.
[3] A.W. Kleyn, Chemical Society Reviews, **32** (2003) 87-95.
[4] J.R. Manson, Chapter 3 Energy Transfer to Phonons in Atom and Molecule Collisions with Surfaces, in: E. Hasselbrink, B.I. Lundqvist (Eds.) Handbook of Surface Science, Elsevier, Amsterdam, 2008, pp. 53-93.
[5] A.W. Kleyn, Chapter 2 Basic Mechanisms in Atom-Surface Interactions, in: E. Hasselbrink, B.I. Lundqvist (Eds.) Handbook of Surface Science, Elsevier, Amsterdam, 2008, pp. 29-52.
[6] R.M. Logan, R.E. Stickney, The Journal of Chemical Physics, **44** (1966) 195-201.
[7] A. Raukema, R.J. Dirksen, A.W. Kleyn, The Journal of Chemical Physics, **103** (1995) 6217-6231.
[8] C.T. Rettner, J.A. Barker, D.S. Bethune, Physical Review Letters, **67** (1991) 2183.
[9] J.C. Tully, The Journal of Chemical Physics, **92** (1990) 680-686.
[10] A.W. Kleyn, T.C.M. Horn, Physics Reports-Review Section of Physics Letters, **199** (1991) 191-230.
[11] B.H. Cooper, C.A. DiRubio, G.A. Kimmel, R.L. McEachern, Nuclear Instruments and Methods in Physics Research Section B: Beam Interactions with Materials and Atoms, **64** (1992) 49-57.
[12] S.R. Kasi, H. Kang, C.S. Sass, J.W. Rabalais, Surface Science Reports, **10** (1989) 1-104.

[13] B. Berenbak, S. Zboray, B. Riedmüller, D.C. Papageorgopoulos, S. Stolte, A.W. Kleyn, Physical Chemistry Chemical Physics, **4** (2002) 68-74.
[14] A. Amirav, M.J. Cardillo, P.L. Trevor, L. Carmay, J.C. Tully, The Journal of Chemical Physics, **87** (1987) 1796-1807.
[15] J.A. Barker, C.T. Rettner, The Journal of Chemical Physics, **97** (1992) 5844-5850.
[16] J.A. Barker, C.T. Rettner, D.S. Bethune, Chemical Physics Letters, **188** (1992) 471-476.
[17] M.D. Ellison, C.M. Matthews, R.N. Zare, The Journal of Chemical Physics, **112** (2000) 1975-1983.
[18] W.J. Hays, W.E. Rodgers, E.L. Knuth, The Journal of Chemical Physics, **56** (1972) 1652-1657.
[19] E. Pollak, S. Miret-Artés, The Journal of Chemical Physics, **130** (2009) 194710.
[20] M.J. Romney, J.B. Anderson, The Journal of Chemical Physics, **51** (1969) 2490-2496.
[21] H.F. Winters, H. Coufal, C.T. Rettner, D.S. Bethune, Physical Review B, **41** (1990) 6240-6256.
[22] D. Kulginov, M. Persson, C.T. Rettner, D.S. Bethune, The Journal of Physical Chemistry, **100** (1996) 7919-7927.
[23] R.J.W.E. Lahaye, A.W. Kleyn, S. Stolte, S. Holloway, Surface Science, **338** (1995) 169-182.
[24] R.J.W.E. Lahaye, S. Stolte, A.W. Kleyn, R.J. Smith, S. Holloway, Surface Science, **307-309** (1994) 187-192.
[25] A. Amirav, M.J. Cardillo, Physical Review Letters, **57** (1986) 2299.
[26] C. Lim, J.C. Tully, A. Amirav, P. Trevor, M.J. Cardillo, The Journal of Chemical Physics, **87** (1987) 1808-1816.
[27] P.S. Weiss, A. Amirav, P.L. Trevor, M.J. Cardillo, Journal of Vacuum Science & Technology a-Vacuum Surfaces and Films, **6** (1988) 889-894.
[28] K.D. Gibson, S.J. Sibener, H.P. Upadhyaya, A.L. Brunsvold, J. Zhang, T.K. Minton, D. Troya, The Journal of Chemical Physics, **128** (2008) 224708.
[29] M.B. Någård, P.U. Andersson, N. Marković, J.B.C. Pettersson, The Journal of Chemical Physics, **109** (1998) 10339-10349.
[30] Y. Watanabe, H. Yamaguchi, M. Hashinokuchi, K. Sawabe, S. Maruyama, Y. Matsumoto, K. Shobatake, Chemical Physics Letters, **413** (2005) 331-334.
[31] Y. Watanabe, H. Yamaguchi, M. Hashinokuchi, K. Sawabe, S. Maruyama, Y. Matsumoto, K. Shobatake, European Physical Journal D, **38** (2006) 103-109.
[32] D.A. Butler, B. Berenbak, S. Stolte, A.W. Kleyn, Physical Review Letters, **78** (1997) 4653-4656.
[33] E.K. Schweizer, C.T. Rettner, Physical Review Letters, **62** (1989) 3085.
[34] E.K. Schweizer, C.T. Rettner, S. Holloway, Surface Science, **249** (1991) 335-349.
[35] W.W. Hayes, H. Ambaye, J.R. Manson, Journal of Physics-Condensed Matter, **19** (2007) 305007.
[36] W.W. Hayes, H. Ambaye, J.R. Manson, Journal of Physics-Condensed Matter, **20** (2008) 219801.
[37] W.W. Hayes, J.R. Manson, Physical Review B, **75** (2007) 113408.
[38] W.W. Hayes, J.R. Manson, Physical Review B, **77** (2008) 089904.
[39] F. Gou, M.A. Gleeson, J. Villette, A.W. Kleyn, Vacuum, **81** (2006) 196-201.
[40] A. Raukema, Dynamics of Chemisorption, in, University of Amsterdam, 1995.
[41] R.P. Dahiya, M.J. de Graaf, R.J. Severens, H. Swelsen, M.C.M. van de Sanden, D.C. Schram, Physics of Plasmas, **1** (1994) 2086-2095.

[42] M.C.M. van de Sanden, G.M. Janssen, J.M. de Regt, D.C. Schram, J.A.M. van der Mullen, B. van der Sijde, Review of Scientific Instruments, **63** (1992) 3369-3377.
[43] A. Raukema, A.P. de Jongh, H.P. Alberda, R. Boddenberg, F.G. Giskes, E. de Haas, A.W. Kleyn, H. Neerings, R. Schaafsma, H. Veerman, Measurement Science & Technology, **8** (1997) 253-261.
[44] P. Feulner, D. Menzel, Surface Science, **154** (1985) 465-488.
[45] H. Pfnür, P. Feulner, D. Menzel, The Journal of Chemical Physics, **79** (1983) 4613-4623.
[46] K.C. Janda, J.E. Hurst, C.A. Becker, J.P. Cowin, D.J. Auerbach, L. Wharton, The Journal of Chemical Physics, **72** (1980) 2403-2410.
[47] M.E.M. Spruit, E.W. Kuipers, F.H. Geuzebroek, A.W. Kleyn, Surface Science, **215** (1989) 421-436.
[48] M. Lindroos, H. Pfnür, P. Feulner, D. Menzel, Surface Science, **180** (1987) 237-251.
[49] Y.-K. Sun, W.H. Weinberg, Surface Science, **214** (1989) L246-L252.
[50] B. Riedmüller, I.M. Ciobîca, D.C. Papageorgopoulos, F. Frechard, B. Berenbak, A.W. Kleyn, R.A. van Santen, The Journal of Chemical Physics, **115** (2001) 5244-5251.
[51] M. Head-Gordon, J.C. Tully, H. Schlichting, D. Menzel, The Journal of Chemical Physics, **95** (1991) 9266-9276.
[52] E.R. Jones, J.T. McKinney, M.B. Webb, Physical Review, **151** (1966) 476.
[53] E.A. Soares, G.S. Leatherman, R.D. Diehl, M.A. Van Hove, Surface Science, **468** (2000) 129-136.
[54] D.C. Papageorgopoulos, B. Berenbak, M. Verwoest, B. Riedmüller, S. Stolte, A.W. Kleyn, Chemical Physics Letters, **305** (1999) 401-407.
[55] H.H. Brongersma, M. Draxler, M. de Ridder, P. Bauer, Surface Science Reports, **62** (2007) 63-109.
[56] H. Niehus, W. Heiland, E. Taglauer, Surface Science Reports, **17** (1993) 213-303.
[57] D. Menzel, W. Brenig, T. Brunner, W. Frieß, H. Schlichting, Journal of Electron Spectroscopy and Related Phenomena, **64-65** (1993) 583-590.
[58] J. Braun, K.L. Kostov, G. Witte, L. Surnev, J.G. Skofronick, S.A. Safron, C. Wöll, Surface Science, **372** (1997) 132-144.
[59] G.A. Somorjai, Introduction to Surface Chemistry and Catalysis, Wiley, New York 1994.
[60] C. Kittel, Introduction to solid state physics, 8th ed. ed., Wiley, Hoboken, NJ :, 2005.
[61] G.T. Furukawa, M.L. Reilly, J.S. Gallagher, Journal of Physical and Chemical Reference Data, **3** (1974) 163-209.
[62] H.R. Schober, P.H. Dederichs, Metals: Phonon States, Electron States and Fermi Surfaces: Phonon States of Elements. Electron States and Fermi Surfaces of Alloys in: K.H. Hellwege, J.L. Olsen (Eds.) Metals: Phonon States, Electron States and Fermi Surfaces, 1981, pp. 130.
[63] A.D. Tenner, K.T. Gillen, T.C.M. Horn, J. Los, A.W. Kleyn, Physical Review Letters, **52** (1984) 2183.
[64] J.M. Moix, E. Pollak, S. Miret-Artés, Physical Review Letters, **104** (2010) 116103.
[65] C. Bromberger, H.J. Jänsch, D. Fick, Surface Science, **506** (2002) 129-136.
[66] M. Chelvayohan, C.H.B. Mee, Journal of Physics C: Solid State Physics, **15** (1982) 2305.

[67] R.J.W.E. Lahaye, S. Stolte, S. Holloway, A.W. Kleyn, Surface Science, **363** (1996) 91-99.
[68] R. Heid, K.P. Bohnen, Physics Reports, **387** (2003) 151-213.
[69] R. Heid, K.P. Bohnen, T. Moritz, K.L. Kostov, D. Menzel, W. Widdra, Physical Review B, **66** (2002) 161406.